

IMPROVED MULTIEDGE DETECTION AND REFLECTIVITY ESTIMATION FOR SAR IMAGES

Marie Chabert^a, Franz Hlawatsch^b, and Jean-Yves Tournet^a

^aENSEEIH/TéSA, National Polytechnic Institute of Toulouse
2 Rue Camichel, BP 7122, 31071 Toulouse Cedex 7, France
phone: +33 5 61 58 84 76, fax: +33 5 61 58 80 14, email: marie.chabert@tesa.prd.fr

^bInstitute of Communications and Radio-Frequency Engineering, Vienna University of Technology
Gusshausstrasse 25/389, A-1040 Vienna, Austria
email: fhlawats@pop.tuwien.ac.at, web: http://www.nt.tuwien.ac.at/dspgroup/time.html

ABSTRACT

We propose sliding-window multiedge detectors and reflectivity estimators for complex SAR images. The novel detectors and estimators allow to take into account additive observation noise and colored signal (speckle) and noise processes; furthermore, they employ an exponential data weighting to improve spatial resolution. In the multiedge case, simulation results demonstrate a substantial performance improvement over existing methods when the speckle is colored and additive noise is present.

1. INTRODUCTION

The problem of edge detection in synthetic aperture radar (SAR) images has received much attention (see [1–5] and references therein). Because of the multiplicative speckle noise, most standard edge detectors perform poorly when applied to SAR images. Recently, two interesting SAR edge detectors have been proposed in [3, 5].

This paper proposes sliding-window techniques for multiedge detection and reflectivity estimation in complex¹ SAR images. The proposed techniques are based on the generalized likelihood-ratio test (GLRT) and maximum-likelihood (ML) principles, with certain approximations to reduce computational complexity. They improve on existing methods [3, 5] in that they

- allow to take into account additive observation noise (which is usually neglected in conventional SAR image edge detectors) as well as colored signal (speckle) and noise processes,
- and employ an exponential data weighting to improve spatial resolution in the case of multiple edges.

The paper is organized as follows. Section 2 explains the basic sliding-window estimation-detection strategy. In Section 3, the ML reflectivity estimator is derived and a simplified estimator is developed. Section 4 presents the GLRT as well as simplified multiedge detectors. Finally, Section 5 provides simulation results that compare the performance of the proposed estimators and detectors to that of the methods in [3, 5].

2. SOME FUNDAMENTALS

A given line² (or column) of the complex reflectivity SAR image corresponding to the k th look will be modeled as

$$z_k[n] = \sqrt{R[n]} s_k[n] + v_k[n], \quad k = 1, 2, \dots, K, \quad (1)$$

where $R[n] > 0$ is the reflectivity function, $s_k[n]$ is the k th speckle

¹Funding by FWF grant P11904-TEC.

²The complex radar reflectivity of the scene constitutes the primary geophysical data [4] and thus contains a maximum of information. Working directly on the complex image (rather than, e.g., on the intensity image derived from it) allows to derive improved statistical tests [5].

³The present study focuses on the detection of vertical edges. However, two-dimensional implementations similar to those presented in [3, 5] can easily be developed using the proposed methodology.

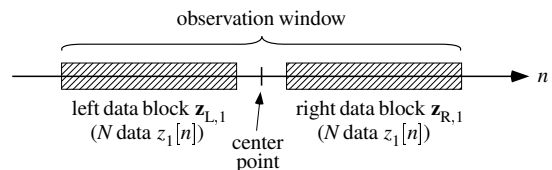


Fig. 1: Sliding-window estimation-detection strategy. For simplicity, only the first look ($k = 1$) is shown.

signal, $v_k[n]$ is the k th additive noise component, and K is the number of looks. The reflectivity function $R[n]$ is modeled as piecewise constant; the multiedge detection problem considered here is precisely the detection of the positions n where $R[n]$ changes its value. All speckle signals $s_k[n]$ and additive noise sequences $v_k[n]$ are statistically independent, circularly complex (and, thus, zero-mean), stationary, Gaussian random processes. Their autocorrelations $r_s[m] = E\{s_k[n+m]s_k^*[n]\}$ and $r_v[m] = E\{v_k[n+m]v_k^*[n]\}$ are the same for all looks and are assumed known. The speckle signals $s_k[n]$ are normalized as $\sigma_s^2 = E\{|s_k[n]|^2\} = r_s[0] = 1$.

Sliding-window strategy. The sliding-window estimation-detection strategy is illustrated in Fig. 1. An observation window slides along a given image line; at each window position, the presence/absence of an edge (i.e., a jump of $R[n]$) at the center point is detected. To this end, the detector computes a reflectivity estimate \hat{R}_L from the K left data blocks $\mathbf{z}_{L,k}$ and a reflectivity estimate \hat{R}_R from the K right data blocks $\mathbf{z}_{R,k}$ ($k = 1, 2, \dots, K$). Within the k th look and for each window position, the left and right data blocks contain N data $z_k[n]$ each; they are separated by a small gap so that the respective data are (effectively) statistically independent.

Evidently, the “left” estimate \hat{R}_L and the “right” estimate \hat{R}_R can be expected to be similar (different) when an edge is absent (present). Therefore, edge detection can be based on a comparison of \hat{R}_L and \hat{R}_R . (As we will demonstrate in Section 4, this detection strategy is also used by the GLRT when the position of the potential edge is considered fixed at the center point.) As the observation window slides along the image line, multiple edges can be detected one after another provided they are not too close.

Reference methods. When the additive noise $v_k[n]$ is neglected ($\sigma_v^2 = 0$), the GLRT allows a simple formulation that has been derived in [5]. The GLRT test statistic here is

$$\mu(r) \triangleq \max \left\{ r, \frac{1}{r} \right\} \quad \text{with } r \triangleq \frac{\hat{R}_L}{\hat{R}_R}, \quad (2)$$

where \hat{R}_L and \hat{R}_R are the “left” and “right” ML estimate, respectively, for the case $\sigma_v^2 = 0$ (see equation (7) for a closed-form expression of \hat{R}_L and \hat{R}_R). The GLRT then decides the presence (absence) of an edge if $\mu(r)$ is above (below) a predefined threshold.

A second SAR edge detection method [3] uses the test statistic in (2) with estimates \hat{R}_L and \hat{R}_R that are obtained by a local filtering of the *intensity* image (the squared magnitude of the complex data $z_k[n]$). The filtering leads to improved spatial resolution in the case of multiple edges.

These two existing methods will be considered as reference methods with which our proposed methods will be compared; they will be discussed in more detail further below. Neither of these reference methods takes into account additive observation noise, although the additive noise can be relatively high in SAR applications. Furthermore, only the first reference method takes into account colored speckle.

3. REFLECTIVITY ESTIMATORS

In this section, we derive the ML reflectivity estimator in the presence of additive observation noise and for arbitrary signal (speckle) and noise correlation functions. We also propose a simplified estimator and a data weighting scheme, calculate the Cramér-Rao lower bound, and review the reference estimators from [3, 5].

For reflectivity estimation, we consider data blocks \mathbf{z}_k of length N each (here, \mathbf{z}_k is either $\mathbf{z}_{L,k}$ or $\mathbf{z}_{R,k}$ and $k = 1, 2, \dots, K$). The derivation of the ML estimator will be based on the assumption that the reflectivity $R[n]$ is locally constant over the signal block. Thus, (1) becomes $z_k[n] = \sqrt{R} s_k[n] + v_k[n]$, with n in the block interval. This can be written in obvious vector notation as

$$\mathbf{z}_k = \sqrt{R} \mathbf{s}_k + \mathbf{v}_k, \quad k = 1, 2, \dots, K.$$

The covariance matrix of \mathbf{z}_k is given by

$$\mathbf{C}_{z_k} = \mathbf{C}_z = R \mathbf{C}_s + \mathbf{C}_v = R \mathbf{C}_s + \sigma_v^2 \bar{\mathbf{C}}_v,$$

where \mathbf{C}_s and \mathbf{C}_v are the covariance matrices of \mathbf{s}_k and \mathbf{v}_k , respectively. For later convenience, we write $\mathbf{C}_v = \sigma_v^2 \bar{\mathbf{C}}_v$, where $\sigma_v^2 = r_v[0]$ is the variance of $v_k[n]$ and the diagonal elements of $\bar{\mathbf{C}}_v$ are 1. All covariance matrices are $N \times N$ Hermitian Toeplitz matrices and do not depend on k . The first column of \mathbf{C}_s is given by $(r_s[0], r_s[1], \dots, r_s[N-1])^T$, and similarly for $\bar{\mathbf{C}}_v$.

Due to the statistical independence and Gaussianity of the data vectors \mathbf{z}_k , the log-likelihood function of R using the overall data vector $\mathbf{z} \triangleq (\mathbf{z}_1^T \mathbf{z}_2^T \dots \mathbf{z}_K^T)^T$ is given by³

$$\ln f(\mathbf{z}; R) = \ln \prod_{k=1}^K f(\mathbf{z}_k; R) \cong -K \ln |\mathbf{C}_z| - \sum_{k=1}^K \mathbf{z}_k^H \mathbf{C}_z^{-1} \mathbf{z}_k, \quad (3)$$

where $|\mathbf{C}_z|$ denotes the determinant of \mathbf{C}_z . This depends on R via $\mathbf{C}_z = R \mathbf{C}_s + \sigma_v^2 \bar{\mathbf{C}}_v$.

ML estimator. The ML reflectivity estimator is defined as [6–8]

$$\hat{R}_{\text{ML}}(\mathbf{z}) \triangleq \arg \max_R \ln f(\mathbf{z}; R). \quad (4)$$

To simplify the computation of $\hat{R}_{\text{ML}}(\mathbf{z})$, we will diagonalize \mathbf{C}_z (simultaneous diagonalization of \mathbf{C}_s and $\bar{\mathbf{C}}_v$ [7]). We can write $\mathbf{C}_z = R \mathbf{C}_s + \sigma_v^2 \bar{\mathbf{C}}_v^{1/2} \mathbf{C}_v^{1/2} = \bar{\mathbf{C}}_v^{1/2} (R \mathbf{C}'_s + \sigma_v^2 \mathbf{I}) \bar{\mathbf{C}}_v^{1/2}$, with $\bar{\mathbf{C}}_v^{1/2}$ the positive definite square root of $\bar{\mathbf{C}}_v$ and $\mathbf{C}'_s \triangleq \bar{\mathbf{C}}_v^{-1/2} \mathbf{C}_s \bar{\mathbf{C}}_v^{-1/2}$ the transformed speckle covariance. Inserting into (3) yields

$$\ln f(\mathbf{z}; R) \cong -K \ln |\mathbf{C}'_z| - \sum_{k=1}^K \mathbf{z}'_k{}^H \mathbf{C}'_z{}^{-1} \mathbf{z}'_k, \quad (5)$$

with $\mathbf{C}'_z \triangleq R \mathbf{C}'_s + \sigma_v^2 \mathbf{I}$ and $\mathbf{z}'_k \triangleq \bar{\mathbf{C}}_v^{-1/2} \mathbf{z}_k$ (here, $\bar{\mathbf{C}}_v^{-1/2}$ acts as a noise whitening filter with respect to the additive noise). Inserting the eigenvalue decomposition of \mathbf{C}'_s , $\mathbf{C}'_s = \mathbf{U} \mathbf{\Lambda} \mathbf{U}^H$ (where $\mathbf{\Lambda}$ is the

diagonal matrix of eigenvalues $\lambda_i \geq 0$ and \mathbf{U} is the unitary eigenvector matrix) into $\mathbf{C}'_z = R \mathbf{C}'_s + \sigma_v^2 \mathbf{I}$ and using $\mathbf{U} \mathbf{U}^H = \mathbf{I}$, we obtain $\mathbf{C}'_z = R \mathbf{U} \mathbf{\Lambda} \mathbf{U}^H + \sigma_v^2 \mathbf{U} \mathbf{U}^H = \mathbf{U} (R \mathbf{\Lambda} + \sigma_v^2 \mathbf{I}) \mathbf{U}^H$. Thus, \mathbf{C}'_z has been diagonalized. Inserting into (5), we readily obtain

$$\ln f(\mathbf{z}; R) \cong - \sum_{i=1}^N \left[K \ln c_i(R) + \frac{v_i(\mathbf{z})}{c_i(R)} \right]. \quad (6)$$

Here, $c_i(R) \triangleq R \lambda_i + \sigma_v^2$ and $v_i(\mathbf{z}) \triangleq \sum_{k=1}^K |\zeta_{k,i}|^2$ where $\zeta_{k,i}$ is the i th element of the vector $\boldsymbol{\zeta}_k \triangleq \mathbf{U}^H \mathbf{z}'_k = \mathbf{U}^H \bar{\mathbf{C}}_v^{-1/2} \mathbf{z}_k$ with (diagonal) covariance $\mathbf{C}'_z = R \mathbf{\Lambda} + \sigma_v^2 \mathbf{I}$. The expression (6) is far simpler to compute than (3). Note also that the eigenvalues λ_i and the data transformation matrix $\mathbf{U}^H \bar{\mathbf{C}}_v^{-1/2}$ can be precomputed. The ML estimator is not exactly unbiased in general but it is asymptotically (as $KN \rightarrow \infty$) unbiased and asymptotically efficient [6–8]. In our simulations, it was effectively unbiased even for small KN .

First reference estimator. In the absence of additive noise ($\sigma_v^2 = 0$), the ML estimator can be shown to simplify to

$$\hat{R}_{\text{ref-1}}(\mathbf{z}) \triangleq \hat{R}_{\text{ML}}(\mathbf{z}) \Big|_{\sigma_v^2=0} = \frac{1}{KN} \sum_{k=1}^K \mathbf{z}_k^H \mathbf{C}_s^{-1} \mathbf{z}_k. \quad (7)$$

This estimator is used in the reference detector (2) [5]. For $\sigma_v^2 = 0$, it is unbiased. However, for $\sigma_v^2 \neq 0$ it has a nonzero bias given by $\frac{\sigma_v^2}{N} \text{tr}\{\mathbf{C}_s^{-1} \bar{\mathbf{C}}_v\} = \frac{\sigma_v^2}{N} \sum_{i=1}^N \frac{1}{\lambda_i}$, where $\text{tr}\{\cdot\}$ denotes matrix trace.

Approximate ML estimator. As a practical alternative to the ML estimator in (4), (6), we propose the following estimator that is obtained by subtracting the bias from $\hat{R}_{\text{ref-1}}(\mathbf{z})$ in (7):

$$\begin{aligned} \hat{R}_{\text{sim}}(\mathbf{z}) &\triangleq \frac{1}{KN} \sum_{k=1}^K \mathbf{z}_k^H \mathbf{C}_s^{-1} \mathbf{z}_k - \frac{\sigma_v^2}{N} \text{tr}\{\mathbf{C}_s^{-1} \bar{\mathbf{C}}_v\} \\ &= \frac{1}{KN} \sum_{i=1}^N \frac{v_i(\mathbf{z}) - K \sigma_v^2}{\lambda_i}. \end{aligned} \quad (8)$$

This estimator is unbiased even for $\sigma_v^2 \neq 0$. For small σ_v^2 , it provides an approximation to the ML estimator although it is much simpler to compute (hence the subscript *sim*).

Second reference estimator. As a final estimator, we consider the estimator that is used by the second reference detector mentioned at the end of Section 2 [3]. Extended to the multiple-look case considered here, this estimator is given by

$$\hat{R}_{\text{ref-2}}(\mathbf{z}^w) \triangleq \frac{1}{K} \sum_{k=1}^K \sum_{m=1}^N g[m] |z_k[n_0 + m - 1]|^2$$

(the superscript w will become clear presently). Here, n_0 is the start time of the data block (hereafter we set $n_0 = 1$ for simplicity) and $g[m]$ is an exponential impulse response. $\hat{R}_{\text{ref-2}}(\mathbf{z})$ can be written as

$$\hat{R}_{\text{ref-2}}(\mathbf{z}^w) = \frac{1}{KN} \sum_{k=1}^K \sum_{n=1}^N |z_k^w[n]|^2, \quad (9)$$

with the *weighted data* $z_k^w[n] \triangleq h[n] z_k[n]$ where $h[n] = \sqrt{N g[n]}$. If $g[n]$ is an exponential function, then so is $h[n]$.

Data weighting. We will now extend this data weighting to our estimators $\hat{R}_{\text{ML}}(\mathbf{z})$ and $\hat{R}_{\text{sim}}(\mathbf{z})$. The goal is to improve the spatial resolution (i.e., ability to detect closely spaced multiple edges) of the edge detectors using these estimators. As illustrated in Fig. 2, the weighting emphasizes (deemphasizes) data samples located near (away from) the center point, thereby reducing the estimator's sensitivity to edges within the observation window that are located

³The symbol \cong means “effectively equal;” it is used because we suppress all irrelevant terms of $\ln f(\mathbf{z}; R)$ that do not depend on R .

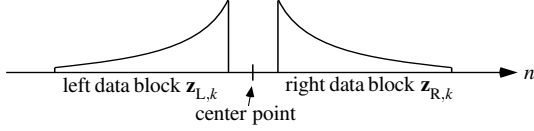


Fig. 2: Exponential data weighting for the k th look.

away from the center point. The price paid is an increase of the estimator's variance which, however, is not dramatic in typical cases.

The right data block of the k th look, $\mathbf{z}_{R,k}$, is replaced with the weighted vector $\mathbf{z}_{R,k}^w$ whose elements are

$$z_{R,k}^w[n] = \frac{w[n]}{w_0} z_{R,k}[n], \quad n = 1, 2, \dots, N.$$

Here, $w[n] > 0$ is a decreasing weight function (e.g., the exponential function $w[n] = e^{-a(n-1)/N}$ with $a \geq 0$) and w_0 is a normalization constant chosen as⁴ $w_0 = \sqrt{\frac{1}{N} \sum_{n=1}^N w^2[n]}$. For the definition of $\mathbf{z}_{L,k}^w$, the weight function $w[n]$ is time-reversed as shown in Fig. 2. We shall denote an estimator using weighted data as $\hat{R}^w(\mathbf{z}^w)$ or briefly \hat{R}^w . Note that $\hat{R}_{\text{ref-2}}^w(\mathbf{z}^w)$ in (9) can be written as

$$\hat{R}_{\text{ref-2}}^w(\mathbf{z}^w) = \frac{\|\mathbf{z}^w\|^2}{KN}, \quad \text{with } \|\mathbf{z}^w\|^2 \triangleq \sum_{k=1}^K \|\mathbf{z}_k^w\|^2. \quad (10)$$

White processes. When both $s_k[n]$ and $v_k[n]$ are white, i.e., $\mathbf{C}_s = \bar{\mathbf{C}}_v = \mathbf{I}$, the two estimators \hat{R}_{ML} in (4) and \hat{R}_{sim} in (8) coincide,

$$\hat{R}_{\text{ML}}(\mathbf{z}) = \hat{R}_{\text{sim}}(\mathbf{z}) = \frac{\|\mathbf{z}\|^2}{KN} - \sigma_v^2, \quad (11)$$

with $\|\mathbf{z}\|^2 \triangleq \sum_{k=1}^K \|\mathbf{z}_k\|^2$. Thus, in the white case, the standard technique of subtracting the noise power from the reflectivity estimator designed for the noiseless case [2, p. 220] yields the ML estimator. Also, the ML estimator is exactly unbiased in the white case.

Furthermore, in the white case the first reference estimator in (7) simplifies as $\hat{R}_{\text{ref-1}}(\mathbf{z}) = \|\mathbf{z}\|^2/(KN)$, and thus it becomes equal to $\hat{R}_{\text{ML}}(\mathbf{z}) = \hat{R}_{\text{sim}}(\mathbf{z})$ in (11) except for the lack of bias correction. Finally, use of weighted data in $\hat{R}_{\text{ref-1}}(\mathbf{z})$ would make it equal to $\hat{R}_{\text{ref-2}}^w(\mathbf{z}^w)$ in (10), i.e., $\hat{R}_{\text{ref-1}}(\mathbf{z}^w) = \hat{R}_{\text{ref-2}}^w(\mathbf{z}^w)$ in the white case.

Cramér-Rao lower bound. The Cramér-Rao lower bound (CRLB) is a lower bound on the variance of any unbiased estimator \hat{R} [6–8]. Using (6), the CRLB is obtained as

$$\text{var}\{\hat{R}\} \geq \frac{1}{K \sum_{i=1}^N \left(\frac{\lambda_i}{c_i(R)}\right)^2} = \frac{R^2}{K \sum_{i=1}^N \frac{1}{[1 + \sigma_v^2/(R\lambda_i)]^2}}. \quad (12)$$

Thus, the CRLB will be larger for larger R and/or smaller K and/or smaller “SNR terms” $R\lambda_i/\sigma_v^2$.

4. MULTIEDGE DETECTORS

We now apply our estimators to multiedge detection. We will derive the GLRT and two simplified detectors, and we will review the reference detectors from [3, 5]. Hereafter, $\mathbf{z}_L \triangleq (\mathbf{z}_{L,1}^T \mathbf{z}_{L,2}^T \dots \mathbf{z}_{L,K}^T)^T$ and $\mathbf{z}_R \triangleq (\mathbf{z}_{R,1}^T \mathbf{z}_{R,2}^T \dots \mathbf{z}_{R,K}^T)^T$ denote the collected “left” and “right” data, respectively, and $\mathbf{z} \triangleq (\mathbf{z}_L^T \mathbf{z}_R^T)^T$ denotes the total data vector.

GLRT. The GLRT of an edge located at the center point decides between the hypothesis of different reflectivity values R_L and R_R

⁴This choice of w_0 guarantees that (i) $w[n]/w_0 \equiv 1$ for $w[n] \equiv 1$ and (ii) the ML estimator/simplified estimator in the white case (see (11)) remains unbiased when \mathbf{z}_k is replaced by \mathbf{z}_k^w .

on the left and right side, respectively (presence of an edge) and the hypothesis of the same reflectivity R_0 on both sides (absence of an edge). The log-likelihood ratio for these hypotheses is [9]

$$\Lambda(\mathbf{z}; R_0, R_L, R_R) = \ln \frac{f(\mathbf{z}_L; R_L) f(\mathbf{z}_R; R_R)}{f(\mathbf{z}; R_0)},$$

where the statistical independence of the left and right data blocks has been used. It can be shown that

$$\Lambda(\mathbf{z}; R_0, R_L, R_R) = \sum_{i=1}^N \left[K \ln \frac{c_i^2(R_0)}{c_i(R_L) c_i(R_R)} + \left[\frac{1}{c_i(R_0)} - \frac{1}{c_i(R_L)} \right] v_i(\mathbf{z}_L) + \left[\frac{1}{c_i(R_0)} - \frac{1}{c_i(R_R)} \right] v_i(\mathbf{z}_R) \right].$$

Because R_0 , R_L , and R_R are unknown, the ML estimates (cf. (4), (6)) are used. The GLRT then decides the presence (absence) of an edge if the resulting GLRT test statistic

$$\Lambda_{\text{GLRT}}(\mathbf{z}) \triangleq \Lambda(\mathbf{z}; \hat{R}_{0,\text{ML}}(\mathbf{z}), \hat{R}_{L,\text{ML}}(\mathbf{z}_L), \hat{R}_{R,\text{ML}}(\mathbf{z}_R))$$

is above (below) a predefined threshold.

When both $s_k[n]$ and $v_k[n]$ are white, $\Lambda_{\text{GLRT}}(\mathbf{z})$ can be shown to be equivalent (up to a transformation of the threshold) to

$$\mu(r_w) = \max \left\{ r_w, \frac{1}{r_w} \right\} \quad \text{with } r_w \triangleq \frac{\|\mathbf{z}_L\|^2}{\|\mathbf{z}_R\|^2}.$$

First reference detector. In the absence of additive noise ($\sigma_v^2 = 0$), the GLRT test statistic can be shown to be equivalent (up to a transformation of the threshold) to (2), i.e.,

$$\mu(r_{\text{ref-1}}) = \max \left\{ r_{\text{ref-1}}, \frac{1}{r_{\text{ref-1}}} \right\} \quad \text{with } r_{\text{ref-1}} \triangleq \frac{\hat{R}_{L,\text{ref-1}}(\mathbf{z}_L)}{\hat{R}_{R,\text{ref-1}}(\mathbf{z}_R)}, \quad (13)$$

where $\hat{R}_{L,\text{ref-1}}(\mathbf{z}_L)$ and $\hat{R}_{R,\text{ref-1}}(\mathbf{z}_R)$ are the left and right versions of the first reference estimator in (7) [5].

Approximate GLRTs. For reasonably good SNR, the ML estimators in $\Lambda_{\text{GLRT}}(\mathbf{z}) = \Lambda(\mathbf{z}; \hat{R}_{0,\text{ML}}(\mathbf{z}), \hat{R}_{L,\text{ML}}(\mathbf{z}_L), \hat{R}_{R,\text{ML}}(\mathbf{z}_R))$ can be replaced with the corresponding simplified estimators $\hat{R}_{0,\text{sim}}(\mathbf{z})$, $\hat{R}_{L,\text{sim}}(\mathbf{z}_L)$, and $\hat{R}_{R,\text{sim}}(\mathbf{z}_R)$ in (8); this leads to the test statistic

$$\Lambda_{\text{sim}}(\mathbf{z}) \triangleq \Lambda(\mathbf{z}; \hat{R}_{0,\text{sim}}(\mathbf{z}), \hat{R}_{L,\text{sim}}(\mathbf{z}_L), \hat{R}_{R,\text{sim}}(\mathbf{z}_R)).$$

An even stronger simplification can be obtained by using the test statistic $\mu(\cdot)$ (cf. (13)) together with the simplified estimators, i.e.,

$$\mu(r_{\text{sim}}) = \max \left\{ r_{\text{sim}}, \frac{1}{r_{\text{sim}}} \right\} \quad \text{with } r_{\text{sim}} \triangleq \frac{\hat{R}_{L,\text{sim}}(\mathbf{z}_L)}{\hat{R}_{R,\text{sim}}(\mathbf{z}_R)}.$$

Note that both Λ_{sim} and $\mu(r_{\text{sim}})$ are equivalent to the GLRT test statistic Λ_{GLRT} when $\sigma_v^2 = 0$, and they will approximate Λ_{GLRT} for small σ_v^2 . To improve spatial resolution, we shall use an exponential data weighting as discussed in Section 3; the resulting test statistics will be denoted by Λ_{sim}^w and $\mu(r_{\text{sim}}^w)$.

Second reference detector. Using the test statistic $\mu(\cdot)$ with the second reference estimator in (9), (10) yields

$$\mu(r_{\text{ref-2}}^w) = \max \left\{ r_{\text{ref-2}}^w, \frac{1}{r_{\text{ref-2}}^w} \right\} \quad \text{with } r_{\text{ref-2}}^w \triangleq \frac{\hat{R}_{L,\text{ref-2}}^w(\mathbf{z}_L^w)}{\hat{R}_{R,\text{ref-2}}^w(\mathbf{z}_R^w)}.$$

Note that this test statistic already incorporates an exponential data weighting.

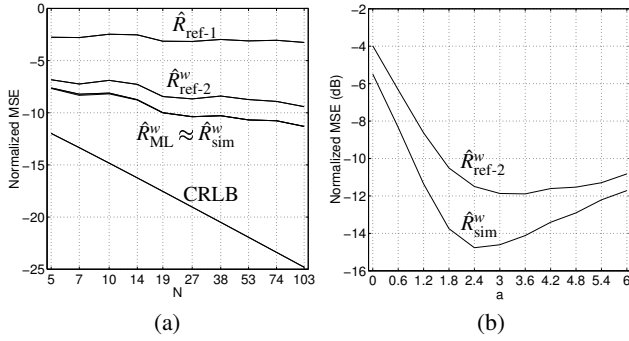


Fig. 3: Performance of reflectivity estimators. (a) Normalized MSE vs. data-block length N , (b) Normalized MSE vs. weighting parameter a .

5. SIMULATION RESULTS

We finally use numerical simulations to compare the performance of our methods to that of the reference methods from [3, 5].

Estimators. We first compare the proposed estimators $\hat{R}_{\text{ML}}(\mathbf{z}^w)$ and $\hat{R}_{\text{sim}}(\mathbf{z}^w)$ to the reference estimators $\hat{R}_{\text{ref-1}}(\mathbf{z})$ and $\hat{R}_{\text{ref-2}}(\mathbf{z}^w)$. The signal (speckle) is a Gaussian AR(2) process [10, 11] with AR parameter vector $[1, 0.2, 0.7]$; the additive noise is white Gaussian. The reflectivity is $R = 10$ on the left side and up to the center of the right side where it changes to $R' = 20$ (this corresponds to a “parasitic” edge such as it must be expected to occur in the multi-edge case). The estimators $\hat{R}_{\text{ML}}(\mathbf{z}^w)$, $\hat{R}_{\text{sim}}(\mathbf{z}^w)$, and $\hat{R}_{\text{ref-2}}(\mathbf{z}^w)$ use an exponential data weighting $w[n] = e^{-a(n-1)/N}$ with $a = 1$.

Fig. 3(a) shows the (estimated) normalized MSE $E\{(\hat{R} - R)^2\}/R^2$ versus the data-block length N . The normalized CRLB (cf. (12)) is also shown for comparison.⁵ The SNR R/σ_v^2 is 15 dB. The MSEs are seen to be much larger than the CRLB; this is due to the parasitic edge and, to a smaller extent, to the data weighting. Estimator $\hat{R}_{\text{ref-1}}(\mathbf{z})$ performs significantly worse than the other estimators because the lack of data weighting makes it much more sensitive to the parasitic edge. The MSEs of the proposed estimators $\hat{R}_{\text{ML}}(\mathbf{z}^w)$ and $\hat{R}_{\text{sim}}(\mathbf{z}^w)$ are practically identical; they are smaller than the MSE of $\hat{R}_{\text{ref-2}}(\mathbf{z}^w)$ and much smaller than that of $\hat{R}_{\text{ref-1}}(\mathbf{z})$.

Fig. 3(b) shows the normalized MSE of $\hat{R}_{\text{sim}}(\mathbf{z}^w)$ and $\hat{R}_{\text{ref-2}}(\mathbf{z}^w)$ as a function of the weighting parameter a appearing in $w[n] = e^{-a(n-1)/N}$. The data-block length is $N = 40$; the SNR is 15 dB. The MSE of $\hat{R}_{\text{sim}}(\mathbf{z}^w)$ (respectively of $\hat{R}_{\text{ref-2}}(\mathbf{z}^w)$) is minimal for $a = a_{\text{opt}} \approx 2.4$ (respectively for $a = a_{\text{opt}} \approx 3.3$). Indeed, the parasitic edge introduces a bias that can be reduced by a stronger weighting (i.e., a larger a) at the cost of a larger variance. In this bias-variance tradeoff, there exists an optimal weighting a_{opt} that leads to minimal MSE. The figure demonstrates that a judicious weighting significantly improves estimation results in the case of multiple edges. It also demonstrates that we could achieve better results than those shown in Fig. 3(a) and Fig. 4 for $a = 1$.

Detectors. Next, we compare the performance of the proposed edge detectors Λ_{sim}^w and $\mu(r_{\text{sim}}^w)$ to that of the reference detectors $\mu(r_{\text{ref-1}})$ and $\mu(r_{\text{ref-2}}^w)$. The statistics of speckle and additive noise are as before. The data-block length is $N = 40$, the weighting parameter is $a = 1$, and the SNR is 15 dB. Under hypothesis H_0 (absence of an edge), the reflectivity is $R_0 = 10$ on both sides. Under hypothesis H_1 (presence of an edge), the reflectivity is $R'_L = 40$ up to the middle of the left data block and $R_L = 10$ afterwards; on the right side, it is $R_R = 30$ up to the middle and $R'_R = 15$ afterwards.

⁵Note that for an unbiased estimator as assumed for the CRLB, the variance equals the MSE.

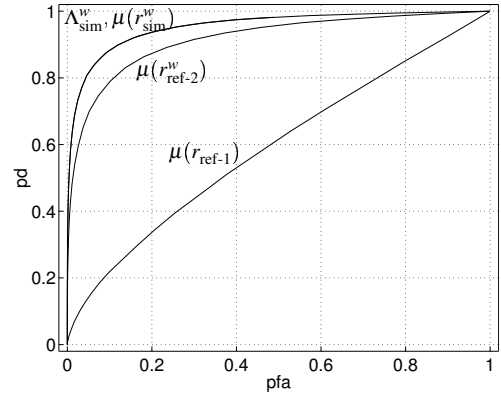


Fig. 4: ROC of multiedge detectors.

Thus, under hypothesis H_1 , there occur both an edge at the center point and parasitic edges at the middle of each data block.

Fig. 4 shows the receiver operating characteristics (ROC) [8] of the various detectors. As expected, the detectors using data weighting significantly outperform $\mu(r_{\text{ref-1}})$ due to their smaller sensitivity to the parasitic edges. The proposed detectors Λ_{sim}^w and $\mu(r_{\text{sim}}^w)$ yield practically identical results. (They were also observed in our experiments to perform very similarly to the GLRT.) They perform better than $\mu(r_{\text{ref-2}}^w)$ and much better than $\mu(r_{\text{ref-1}})$.

6. CONCLUSION

We presented sliding-window multiedge detectors and reflectivity estimators for complex SAR images. These methods are advantageous because they are able to take into account additive observation noise and colored processes, and because they employ a data weighting to improve spatial resolution in the multiedge case. Simulation results demonstrated the good performance of the novel methods. Specifically, the proposed “simplified” estimators and detectors perform as well as the ML estimator and the GLRT, respectively, and better than existing methods.

REFERENCES

- [1] A. C. Bovik, “On detecting edges in speckle imagery,” *IEEE Trans. Acoust., Speech, Signal Processing*, vol. 36, no. 10, pp. 1618–1627, 1988.
- [2] J. C. Curlander and R. N. McDonough, *Synthetic Aperture Radar*. Wiley, 1991.
- [3] R. Fjørtoft, A. Lopès, P. Marthon, and E. Cubero-Castan, “An optimal multiedge detector for SAR image segmentation,” *IEEE Trans. Geosci. and Remote Sensing*, vol. 36, pp. 793–802, May 1998.
- [4] C. J. Oliver and S. Quegan, *Understanding Synthetic Aperture Radar Images*. Artech House, 1998.
- [5] R. Fjørtoft, A. Lopès, J. Bruniquel, and P. Marthon, “Optimal edge detection and edge localization in complex SAR images with correlated speckle,” *IEEE Trans. Geosci. and Remote Sensing*, vol. 37, pp. 2272–2281, Sept. 1999.
- [6] S. M. Kay, *Fundamentals of Statistical Signal Processing: Estimation Theory*. Englewood Cliffs (NJ): Prentice-Hall, 1993.
- [7] C. W. Therrien, *Discrete Random Signals and Statistical Signal Processing*. Englewood Cliffs (NJ): Prentice-Hall, 1992.
- [8] H. L. Van Trees, *Detection, Estimation, and Modulation Theory, Part I: Detection, Estimation, and Linear Modulation Theory*. New York: Wiley, 1968.
- [9] M. Basseville and I. V. Nikiforov, *Detection of Abrupt Changes: Theory and Application*. Englewood Cliffs NJ: Prentice-Hall, 1993.
- [10] P. A. Kelly, H. Derin, and K. D. Hartt, “Adaptive segmentation of speckled images using a hierarchical random field model,” *IEEE Trans. Acoust., Speech, Signal Processing*, vol. 36, no. 10, pp. 1628–1641, 1988.
- [11] J. Y. Tourneret, “Detection and estimation of abrupt changes contaminated by multiplicative gaussian noise,” *Signal Processing*, vol. 68, pp. 259–270, 1998.